AERODYNAMIC PERFORMANCE OF A REMOTELY PILOTED VEHICLE

M. Z. Abdullah, Z. Mohd Ali and Z. Husain

School of Mechanical Engineering, Engineering Campus, Universiti Sains Malaysia, 14300 Nibong Tebal, Seberang Perai Selatan, Penang

ABSTRACT

An experimental investigation and computer simulation have been made to obtain the aerodynamic characteristics of a remotely piloted vehicle (RPV), USM eFA-1. In the present study, the aerodynamic investigations are carried out on a USM eFA-1 RPV. The computational analysis is made on a three-dimensional model of RPV using the computational fluid dynamic (CFD) commercial package FLUENT 6.0. The experimental investigations are carried on a scale model and tested in an open circuit wind tunnel. The investigations have been carried out at three different Reynolds Numbers, i.e. 1.05 x 10^5, 1.26 x 10^5 and 1.60 x 10^5, at different angles of attack. The results show that the lift and drag coefficients increase with increase in the angle of attack. The maximum lift coefficient that can be achieved by the RPV is 0.888 and the minimum drag coefficient is 0.037. The stall angle occurs at angle of attack of α=14°. The simulation result shows fairly good agreement with the experimental result. The results provide an aerodynamic database of the USM eFA-1 RPV for future use.

Keywords : *Drag, k-ε Model, Lift, Remotely Piloted Vehicle, Reynolds Number*

INTRODUCTION

The remotely piloted vehicle (RPV) or unmanned aerial vehicle (UAV) is a small aircraft that is remotely controlled by human from the ground. In civil application, the RPV is becoming very important due to its capability, in terms of avoiding human risks in hazardous environments, high on-board safety, unlimited operational endurance, etc. [1-4]. The RPV has been used in different applications such as remote sensing, weather observation, smuggling activity prevention etc. Moreover, the advances in telecommunications, microelectronics and micro sensors give RPV an enormous potential in a wide variety of scenarios. It has been shown that RPV can be more profitable than their competitors, mainly light airplanes and helicopters, although the development and acquisition cost may be high [5].

The maturing of UAV capabilities has been discussed by Wong et al. [6]. Many research works to date have produced promising results towards the development of fully autonomous capabilities for UAV and has brought the core autonomous flight control system to an advanced state of development. The characteristics study of static longitudinal and lateral-directional stability and control was conducted by Howard et al. [7]. A half scale model based on the real remotely piloted vehicle was used. A Pioneer system was instrumented to measure the control surface deflection, angle of attack, side slip angle and airspeed. Tests were conducted in a wind tunnel and numerical studies were made using low order panel method to validate the experimental results. The results of the longitudinal flight testing indicated that the static margin of Pioneer system was sufficient to open the restricted center of gravity (C.G) envelope. The experimental results agreed well with the computer simulation. The lateral-directional tests indicated limiting control surface on the rudder when compensating for crosswind condition. Howard also suggested that a low cost scaled model flight test is needed in order to provide the aerodynamic data [7].

Jacob [8] carried out the studies on the fluid dynamics of adaptive airfoils. Adaptive wings are the wings wherein shapes can be altered in flight and have a promise in revolutionising aeronautics. The primary motive for altering wing geometry is to improve airfoil efficiency in off-design flight regimes. In his discussion about the application of adaptive wings, Jacob recommended the application of adaptive wing in RPV and UAV. It is due to the fact that RPV and UAV have varied mission goals such as loiter, encounter and rapid return where the vehicle has to perform a variety of flight regime. An adaptive wing would be an ideal lifting system for such a vehicle and it would be possible to retrofit an existing UAV with an adaptive wing.

The preliminary design of a low speed, long endurance remote piloted vehicle for civil application were carried out by Martinez–Val and Hernandez [5]. The objective of the study was to describe the major features of an unmanned air vehicle, designed under very severe safety and performance requirements for missions of surveillance of borders and coast, fire detection, and search and rescue. Due to safety reasons, two engines were mandatory for the aircraft. The design covers the common area: configuration and sizing, aerodynamics, performance, stability and control, airworthiness and initial structural design. Apart from that Martinez-Val and Hernandez also found out that a composite material made the airframe light and strong to achieve the designed goals.

In the present study, experimental investigation and computer simulation have been made on USM eFA1 remotely piloted vehicle in order to obtain the aerodynamic characteristics of the aircraft. The USM eFA1 remotely piloted vehicle has been designed at the Universiti Sains Malaysia (USM) and fabricated in Indonesia for the aerial photographic and remote sensing applications.

DEVELOPMENT OF USM EFA-1 RPV SYSTEM

The RPV has been built as a technology demonstrator and as a research platform for supporting research activities in the Universiti Sains Malaysia. The first prototype called USM eFA-1 has been developed and designed based on simple requirements (Figure 1). RPV will be used to gain insight on the behavior of aerial vehicle during flight mission. The lifting surfaces are designed by considering low flow range of the aircraft. The RPV has been installed with radio control system with FM frequency.

Figure 1: Photograph of the USM eFA-1 RPV

The prototype has been designed to carry the payload of 4kg maximum at cruising altitude of 1000m above sea level. The cruising speed is 100km/h and for about 2 to 3hours of flight. The detail specifications of RPV are tabulated in Table 1.

Table 1: Specification of USM eFA-1 remotely piloted vehicle

Maximum take-off weight	18kg
Payload	4kg
Empty weight	11kg
Fuel weight	3kg
Wing span	3m
Wing aspect ratio (AR)	8
Wing area	1.125m2
Cruising speed	100km/h
Cruising altitude (above sea level)	1000m
Cruising speed	100km/h
Stalling speed (full flapped)	36km/h
Endurance	2 to 3 hours
Take-off distance	100m

The RPV configurations were made as simple as possible for easier fabrication and to minimize cost. It has been tested at the air strip and successfully flew and safely returned back to the base.

EXPERIMENTAL AND COMPUTATIONAL SET-UP

In the present study, the experiments were carried out in the wind tunnel laboratory at the School of Mechanical Engineering, Universiti Sains Malaysia. The schematic diagram of wind tunnel is shown in Figure 2. The wind tunnel is an open type and has a closed test section. The dimension of the test section is 300mm (width) x 300mm (height) x 600mm (length). The basic components of open circuit wind tunnel are intake section, honeycomb intake, contraction section, test section, diffuser, fans and delivery section. The air enters at the intake section. At the contraction section, the nozzle will converge to a smaller area and the velocity is increased at the test section. The air will flow uniformly in the test section and enters into a diverging duct called diffuser.

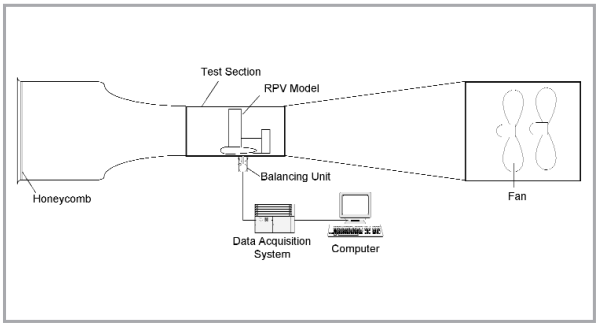

Figure 2: Schematic diagram of the open circuit wind tunnel

The wind tunnel has a maximum speed of 36m/s with a Mach number of 0.1. The turbulence intensity of airflow in the test section is 2.4%. The test equipment includes a three-component electronics-balancing instrument for the measurement of lift, drag and moment forces. The balance was mounted outside of the test section area and connected to a PC. Measurements were taken from an angle of attack of -2° through 16° with an interval of 2°. The fans in the wind tunnel are driven by two electric motors of 3kW.

Figure 3 shows a schematic drawing of RPV model used in the present study. The model has been scaled into 1/5th of its actual size and the main component is made from wood. Fabrication of the model using wood is much easier and also makes the model lighter. The CNC Milling was used in the fabrication process of the model. The boom part is made from aluminium. Aluminium was chosen for its flexibility. The scaled model has an overall dimension of 0.5m in length, 0.158m in height and 0.3m in width. The effects of landing gear, engine propeller, the high lift devices such as flaps and aileron have not been considered in the modelling.

CFD software FLUENT 6.0 and the pre-processor software GAMBIT 1.2 were used in the investigation to predict the lift and drag coefficients. The simulation followed the same condition as that of wind tunnel. Unstructured meshes were used in the modeling. For the turbulence model, the k-ε model was selected in the investigation. The mesh generated around RPV as shown in Figure 4. Initially two different mesh sizes have been used. However, the results are very similar with different of only 0.3 to 0.7%. Thus the smaller mesh number is used for further analysis.

The 'k-ε turbulence model' was used in FLUENT to model the turbulence. The equations describing the relationship between turbulence intensity and turbulence kinetic energy, k and turbulence dissipation rate, ε as follow:

$$k = \frac{3}{2}(U \times TI)^2$$

$$\varepsilon = C_{\mu}^{\frac{3}{4}} \frac{k^{\frac{3}{2}}}{l}$$

where $C_{\mu} = 0.09$
l = turbulence length scale $0.07L$
L = characteristic length

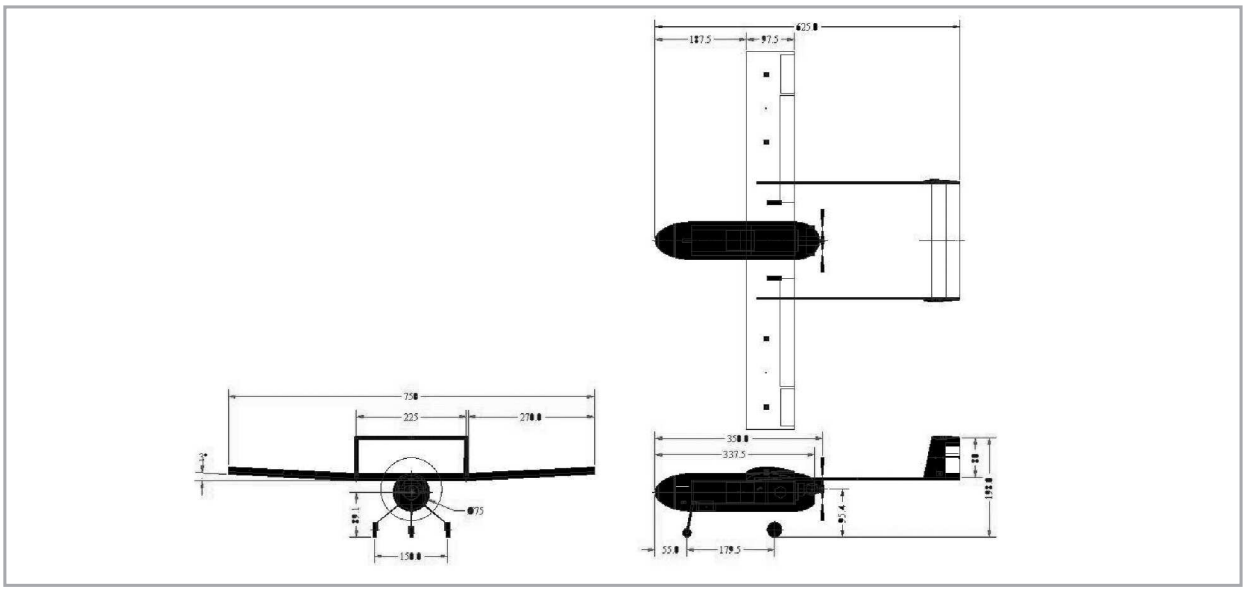

Figure 3: A schematic diagram of RPV model

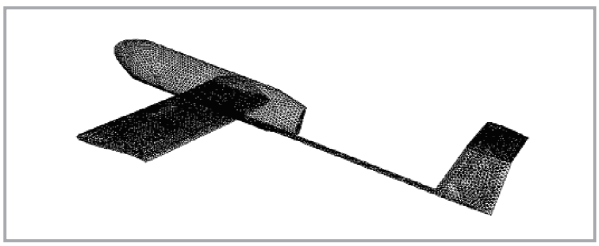

Figure 4: Surface mesh of RPV

U = free stream velocity
TI = turbulence intensity

The aircraft chord is taken as the characteristic length, L.

RESULTS AND DISCUSSION

Figures 5 and 6 present the variation of lift and drag coefficients observed experimentally with respect to the Reynolds number. Figure 5 shows that the lift coefficient curves increasing linearly up to maximum value, i.e. the stall condition. The stall occurred at an angle of attack of 14º for all Reynolds numbers. After the stall, lift coefficient reduced drastically with angle of attacks. The curves for all the Reynolds numbers are similar. The lift curves at Re = 1.60×10^5 is slightly higher than Re = 1.05×10^5 and Re = 1.26×10^5. The lift slope of Re = 1.60×10^5 is 0.066 per degree while Re = 1.26×10^5 and 1.05×10^5 is 0.065 per degree and 0.071 per degree respectively. The lift slope differences are small. Therefore, the results show that Reynolds numbers have no effect on lift coefficient in the range of Reynolds numbers used. Figure 6 shows the drag coefficient curves with respect to the Reynolds numbers. The curves have a minimum drag occurring in a limited range of angle of attack. As the angle of attack increases, C_D increases. The drag curve of Re = 1.60×10^5 is slightly higher compared to that of Re = 1.05×10^5 and Re = 1.26×10^5. However, in general, Reynolds number variation has no effect on drag curves. Therefore, it can be concluded that the Reynolds number does not have much influence on the aerodynamic coefficients for the range of Reynolds numbers tested.

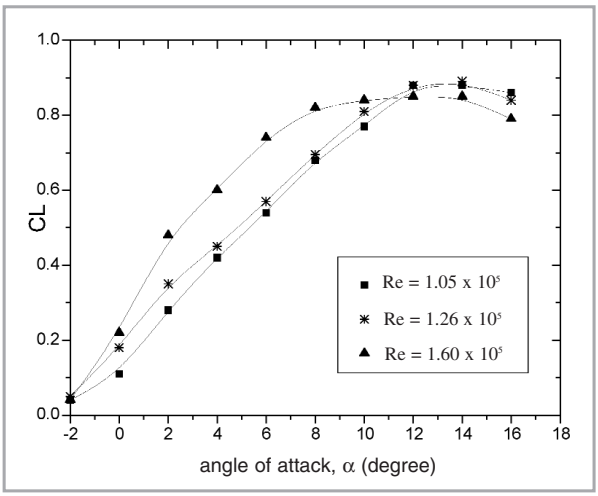

Figure 5: Lift coefficient for different Reynolds Number

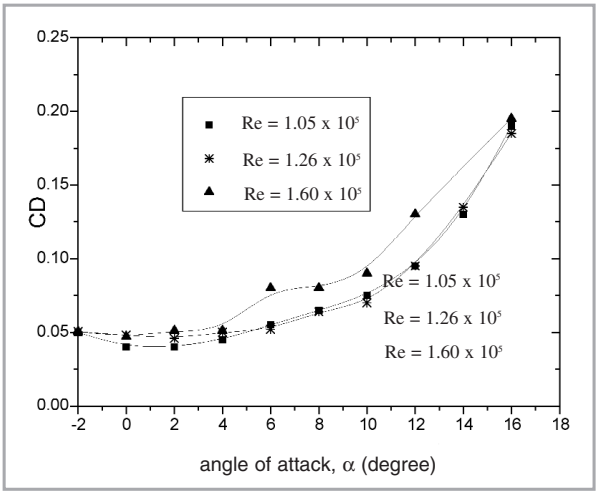

Figure 6: Drag coefficient for different Reynolds Number

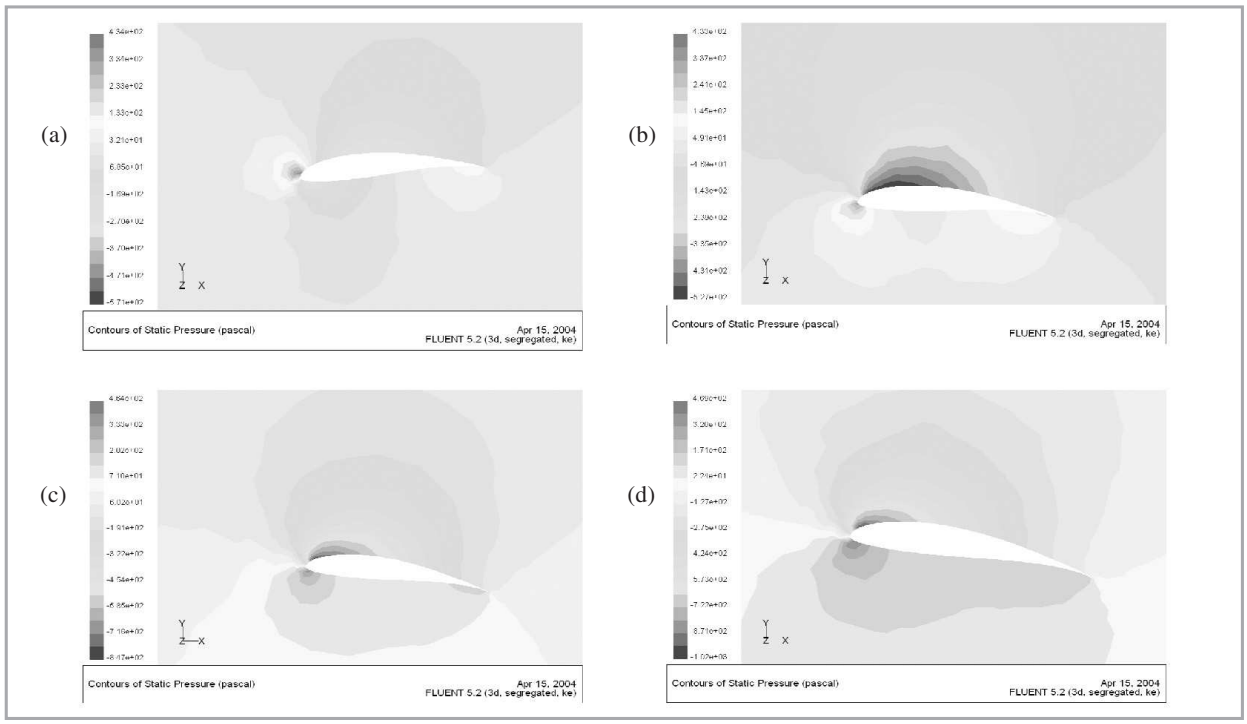

Figures 7(a) – (d): (a) Pressure distribution at α = 0º, (b) Pressure distribution at α = 8º, (c) Pressure distribution at α = 12º, (d) Pressure distribution at α = 14º

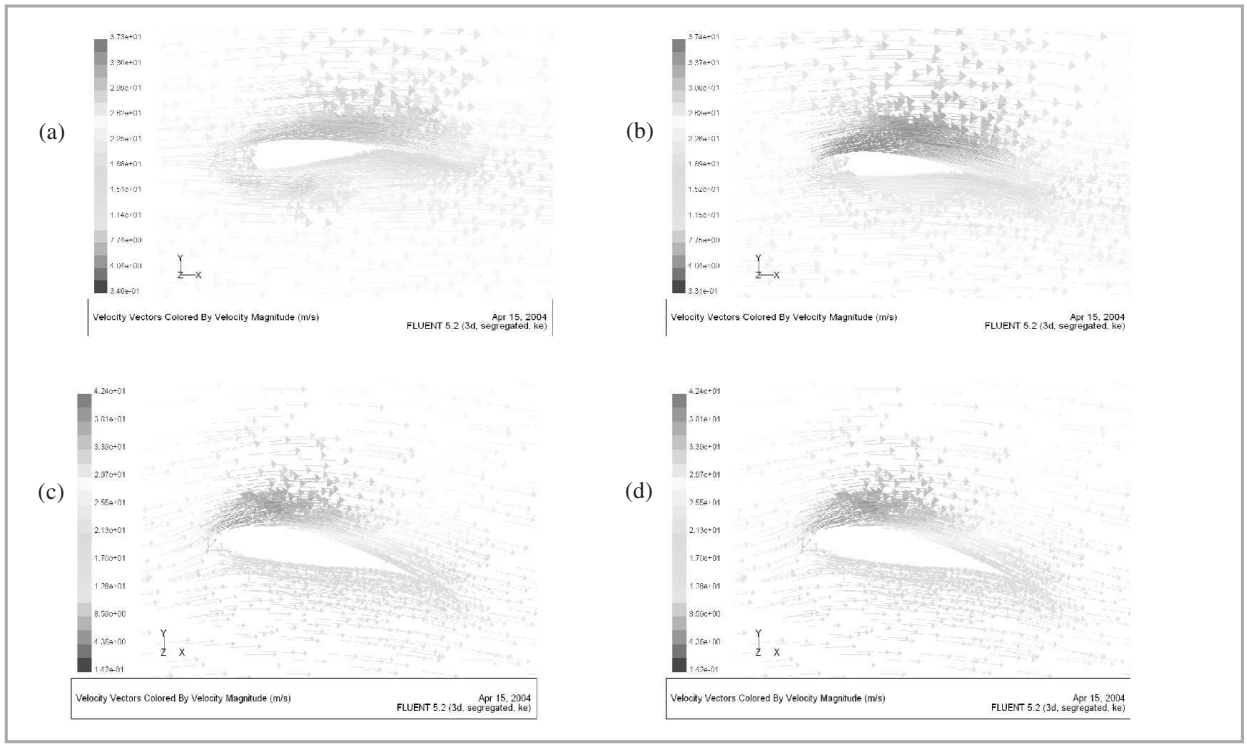

Figures 8(a) - (d): (a) Velocity vector at α = 0º, (b) Velocity vector at α = 8º, (c) Velocity vector at α = 12º, (d) Velocity vector at α = 14º

Figures 7(a) through (d) present the pressure contour around the wing. Figure 7(a) shows the wing pressure contour at $\alpha = 0^{o}$. It is observed the stagnation point is located just above the leading edge. The pressure gradient is observed at the upper surface of the wing. At the lower surface, close to the leading edge the pressure is lower compared to the trailing edge. As the angle is increased to $\alpha = 8^{o}$ (as in Figure 7(b)), the stagnation point moved backward to the lower surface. At the upper surface, the pressure gradient increases. It can be observed that the lowest pressure is near the leading edge. The lowest pressure near the upper surface is 48.8% lower than that in Figure 7(a). At the lower surface, the highest pressure occurs near the leading and trailing edges. At $\alpha = 12^{o}$ in Figure 7(c), the stagnation point moves further backward. At the upper surface, the lowest pressure point moves forward and 39.06% lower compared to that in Figure 7(b). The contour also shows that the pressure gradient increases.

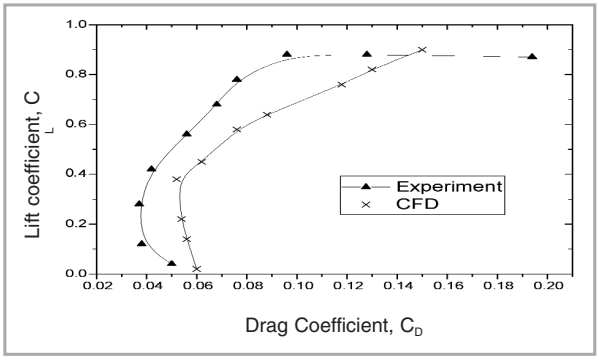

Figure 9: The drag polar curve at Re = 1.05 x 10^5

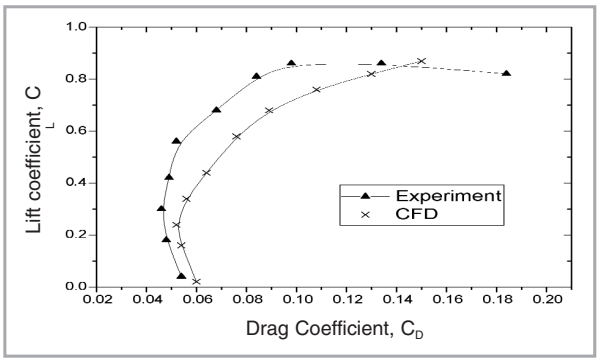

Figure 10: The drag polar curve at Re = 1.26 x 10^5

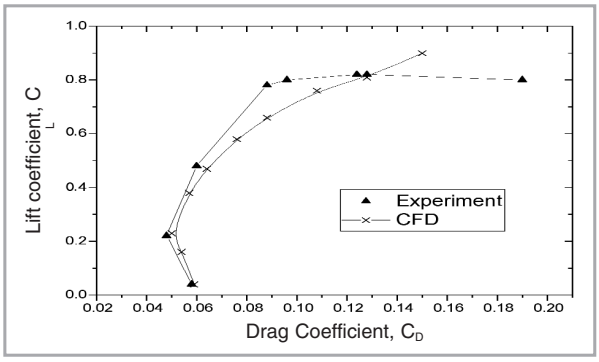

Figure 11: The drag polar curve at Re = 1.60 x 10^5

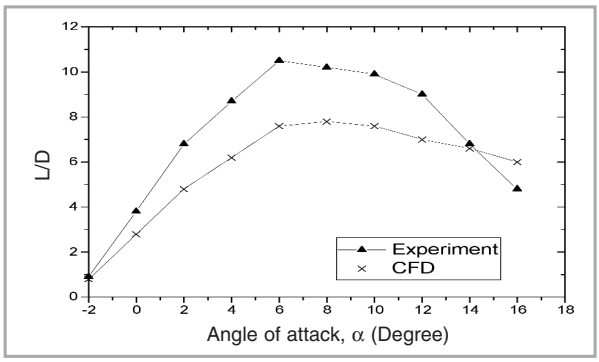

Figure 12: The lift and drag ratio (L/D) against angle of attack (α) at Re = 1.05 x 105

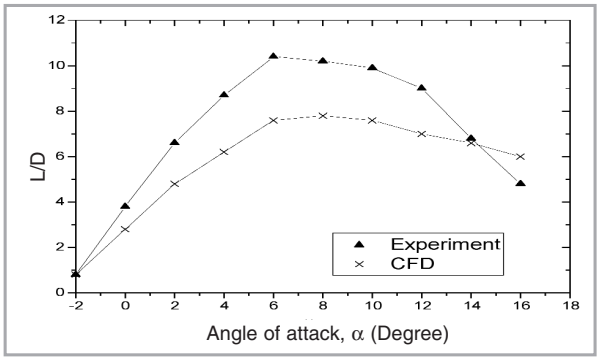

Figure 13: The lift and drag ratio (L/D) against angle of attack (α) at Re = 1.26 x 10^5

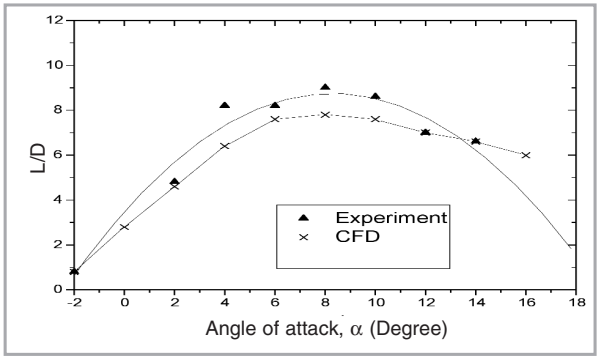

Figure 14: The lift and drag ratio (L/D) against angle of attack (α) at Re = 1.60 x 10^5

The pressure is higher on the lower surface and the highest was observed near the trailing edge. When the angle was increased to $\alpha = 14^{o}$ in Figure 7(d), the stagnation point moved further backward. The upper surface has higher pressure gradient and the lowest pressure point moves forward and 16.88% lower compared to that in Figure 7(c). The pressure on the lower surface is higher and the highest can be observed near the leading and trailing edges. Figures 8(a) through (d) are shown the velocity vectors around the wing will help to understand further for the flows behavior around the wing at different angle of attacks.

The drag polar curves of three Reynolds numbers are represented in Figures 9 through 11. It is observed that experimental drag polar is to the left of computer simulation

and for Re = $1.60x10^6$, both curves almost overlap. The differences of the maximum lift, C_{Lmax} between experimental and simulation results (Figures 9 to 11) are 6.2%, 1.12% and 0.48% respectively.

Figures 12 to 14 show the lift and drag ratio (L/D) against angle of attack for three Reynolds numbers. It is observed that for all figures, the experimental L/D ratio curves are higher than the computer simulation. In Figure 12, L/D_{max} for experimental measurement is 10.45 at $\alpha = 6^o$ and 7.515 at $\alpha = 8^o$ for computer simulation. The same value of L/D_{max} and angle of attack occurs for Re = 1.26×10^6 (Figure 13). Also the L/D_{max} for experimental measurement is 8.57 at $\alpha = 10^o$ and 7.609 at $\alpha = 8^o$ for computer simulation curve for Re = 1.60×10^5.

CONCLUSIONS

The investigations have been carried out using the computational and experimental studies. From the investigation (Re = 1.60×10^5), the lift curve has a highest slope, lowest drag coefficient curve and the highest lift to drag ratio. For the drag polar prediction, lowest drag polar occur at Re = 1.05×10^5.

In the experimental investigation, the stalled phenomenon can be observed. The stall angle occurs at $\alpha = 14^o$ for the Re = 1.05×10^5, 1.26×10^5 and 1.60×10^5. At this angle, the maximum lift coefficient, CLmax is achieved. The CLmax that can be achieved by the eFA-1 RPV is 0.888. After the stall angle, the lift coefficient decreases and the drag coefficient drastically increases. The $C_D$min of the eFA-1 RPV is 0.0365 and occurs at $\alpha = 2^o$. From the drag polar curves, the CLmax occurred at the CD = 0.13. The Reynolds number does not have any effect on aerodynamic characteristics of the RPV, eFA-1 scaled model for the range of Reynolds numbers tested.

The computer simulation has been compared with the experimental results. For all three Reynolds numbers, the experimental result shows higher value compared to the simulation result for the drag polar and lift to drag ratio curves. Thus, fairly good agreements are seen between numerical simulation and experimental results. ■

REFERENCES

[1] Alfissima, F. Basuno, B. and Abdullah, M.Z., *"Design and Development of an Unmanned Aerial Vehicle"*. Proceedings National Conference on AERODYNAMICS AND RELATED TOPICS, pp. 183-190, 2001.

[2] Bluth, R. T., Durkee P. A., Seinfeld, J. H., Flagan, R. C., Russell, L. M., Crowley, P. A. and Finn, P., "Centre for Interdisciplinary *Remotely-Piloted Aircraft Studies (CIRPAS)", Remotely Piloted Vehicle: Thirteen International Conference.* University of Bristol, UK, paper 6, 1998.

[3] Almeida, H., de Brederode, V. and Marcelino, JR., "Aerodynamic Design Analysis and Tests of the Armor X 7UAV", *Remotely Piloted Vehicle: Twelfth International Conference.* University of Bristol, UK, paper5, 1994.

[4] Barlow, J.B. and Chen, W., *"Aerodynamic Characteristics and Control Aspects of a Freewing Tilt-body Airplane"*, *Remotely Piloted Vehicle: Twelfth International Conference.* University of Bristol, UK, paper 14, 1996.

[5] Martinez-Val, R. and Hernàndez, C., *"Preliminary Design of a Low Speed Long Endurance Remote Pilote Vehicle (RPV) For Civil Applications"*. Aircraft Design, vol. 2, pp. 167-182, 1999.

[6] Wong, K.C., Newman, D.M., Gibbens, P.W., Auld, D.J., Wishart , S., Stone, H., Randle, J.A.G., Choong, K.S., Boyle, D.P. and Blythe, P.W., *"Maturing UAV Capabilities – Stepping from Technology Demonstrators to Mission- specific System"*, UAV Activities at Sydney University, pp. 1-12. www.aeromech.usyd.edu.au, 1996.

[7] Howard, R.M., Bray, R.M. and Lyons, D.F., *"Flying-Qualities Analysis of an Unmanned Air Vehicle"*, Journal of Aircraft, vol. 33, pp. 331-336, 1996.

[8] Jacob, J.D., *"On the Fluid Dynamics of Adaptive Airfoils"*, Proceedings of 1998 ASME International Mechanical Engineering Congress and Exposition, pp. 1-10, 1998.

[9] Moelyadi, M.A., *"Wind Tunnel, Aerodynamic Experimental Techniques"*, Bandung: Bandung Institute of Technology, 2001.

PROFILES

Assoc. Prof Dr Mohd. Zulkifly bin Abdullah
School of Mechanical Engineering,
Engineering Campus,
Universiti Sains Malaysia,
14300 Nibong Tebal,
Seberang Perai Selatan, Penang.

Zurriati binti Mohd Ali
Faculty of Mechanical Engineering,
Universiti Institut Teknologi Mara,
Penang Branch,
13500 Permatang Pauh,
Penang.

Zoeb Husain
School of Mechanical Engineering,
Engineering Campus,
Universiti Sains Malaysia,
14300 Nibong Tebal,
Seberang Perai Selatan,
Penang.